RESEARCH ARTICLE

Left Ventricular Remodelling Associated with the Transient Elevated [68Ga]Ga-Pentixafor Activity in the Remote Myocardium Following Acute Myocardial Infarction

Ping Wu[1,2] · Li Xu[1,2] · Qi Wang[3] · Xiaofang Ma[1] · Xinzhu Wang[3] · Hongliang Wang[1,2] · Sheng He[4] · Huibin Ru[1,2] · Yuting Zhao[1] · Yuxin Xiao[1] · Jingying Zhang[1] · Xinchao Wang[2] · Shaohui An[2,5] · Marcus Hacker[6] · Xiang Li[6] · Xiaoli Zhang[7] · Yuetao Wang[8] · Minfu Yang[9] · Zhifang Wu[1,2] · Sijin Li[1,2]

Abstract

Background Previous studies have initially reported accompanying elevated 2-deoxy-2[18F]fluoro-D-glucose ([18F]F-FDG) inflammatory activity in the remote area and its prognostic value after acute myocardial infarction (AMI). Non-invasive characterization of the accompanying inflammation in the remote myocardium may be of potency in guiding future targeted theranostics. [68Ga]Ga-Pentixafor targeting chemokine receptor 4 (CXCR4) on the surface of inflammatory cells is currently one of the promising inflammatory imaging agents. In this study, we sought to focus on the longitudinal evolution of [68Ga]Ga-Pentixafor activities in the remote myocardium following AMI and its association with cardiac function.

Methods Twelve AMI rats and six Sham rats serially underwent [68Ga]Ga-Pentixafor imaging at pre-operation, and 5, 7, 14 days post-operation. Maximum and mean standard uptake value (SUV) and target-to-background ratio (TBR) were assessed to indicate the uptake intensity. Gated [18F]F-FDG imaging and immunofluorescent staining were performed to obtain cardiac function and responses of pro-inflammatory and reparative macrophages, respectively.

Results The uptake of [68Ga]Ga-Pentixafor in the infarcted myocardium peaked at day 5 (all $P = 0.003$), retained at day 7 (all $P = 0.011$), and recovered at day 14 after AMI ($P > 0.05$), paralleling with the rise-fall pro-inflammatory M1 macrophages ($P < 0.05$). Correlated with the peak activity in the infarct territory, [68Ga]Ga-Pentixafor uptake in the remote myocardium on day 5 early after AMI significantly increased (AMI vs. Sham: SUVmean, SUVmax, and TBRmean: all $P < 0.05$), and strongly correlated with contemporaneous EDV and/or ESV (SUVmean and TBRmean: both $P < 0.05$). The transitory remote activity recovered as of day 7 post-AMI (AMI vs. Sham: $P > 0.05$).

Conclusions Corresponding with the peaked [68Ga]Ga-Pentixafor activity in the infarcted myocardium, the activity in the remote region elevated accordingly and led to contemporaneous left ventricular remodelling early after AMI. Further studies are warranted to clarify its clinical application potential.

Keywords [68Ga]Ga-Pentixafor · CXCR4 · Remote myocardium · Inflammation · Acute myocardial infarction · Ventricular remodeling

Abbreviations

PET/CT	Positron emission tomography/computed tomography
AMI	Acute myocardial infarction
CXCR4	C-X-C chemokine receptor 4
SUVmax	Maximum standardized uptake value
SUVmean	Mean standardized uptake value
TBR	Target-to-background ratio
EDV	End-diastolic volume
ESV	End-systolic volume
LVEF	Left ventricular ejection fraction
FDG	Fluorodeoxyglucose
ROI	Regions of interest
CMRI	Cardiac magnetic resonance imaging

Ping Wu and Li Xu contributed equally to this work.

Extended author information available on the last page of the article

Introduction

Acute myocardial infarction (AMI) is one of the leading causes of morbidity and mortality worldwide [1]. Escalated inflammatory cascade response is recognized as a major injury mechanism [2, 3]. Anti-inflammatory strategies specific to the peak inflammatory response after AMI may alleviate left ventricular (LV) improper remodeling [4, 5]. Besides, preclinical studies have shown severe inflammatory response in the infarct territory affect the remote area, which may contribute to adverse LV remodelling and heart failure [6, 7]. Thus, non-invasive and dynamic characteristic assessment of the accompanying inflammation followed by AMI is essentially critical in guiding future targeted theranostics.

2-deoxy-2-[^{18}F]fluoro-D-glucose ([^{18}F]F-FDG) imaging is widely used in clinical practice for the assessment of myocardial viability and cardiac function, when pretreated with heparin, it can also be used to assess myocardial inflammation [8–10]. Given controversial observations of previous studies regarding [^{18}F]F-FDG inflammation in the remote region and the unexpected physiological uptake in the myocardium, other specific inflammatory molecular probes are emerging [10, 11] .

The combination of C-X-C chemokine receptor 4 (CXCR4) and its ligands play a pivotal role in cell migration ("homing"), recruitment, adhesion, growth and proliferation, which was involved in broad-spectrum diseases like hematologic malignancies, more than 30 different types of solid tumors, infectious disease, autoimmune diseases, and et al. [12]. CXCR4 is thus a promising target in the theranostics [13, 14]. More currently, preclinical and clinical studies proved the corresponding novel tracer [^{68}Ga]Ga-Pentixafor can sensitively and non-invasively visualize the expression of CXCR4 on the surface of variety of cells in-vivo [15–17]. Meanwhile, the corresponding radio-targeted therapeutic probes like LY2510924, ^{177}Lu- and ^{90}Y-Pentixather are in active exploration [5, 18].

Most recently, limited preclinical and clinical studies indicated the predictive value of [^{68}Ga]Ga-Pentixafor in the infarcted myocardium, which associated with a wide range of leukocyte subtypes [13, 19, 20]. However, its dynamic evolution in the remote myocardium post AMI and the inflammatory cellular basis are yet to be elucidated currently. In this study, we sought to spy on these questions based on serial cardiac positron emission tomography/computed tomography (PET/CT) scans and histologic methods in AMI rats.

Methods

Animal Model and Experimental Protocols

A total of 12 AMI models and 6 Sham models were successfully established (Fig. 1). Male Sprague-Dawley rats (10–13 weeks old, 280–330 g) were used in order to maintain homogeneity. Rats were anesthetized with 2% isoflurane gas and artificially ventilated (9 ml/kg body weight, 75–85 stroke/min) with an animal ventilator. Twenty μg (0.2 ml) of flurbiprofen axetil was injected intramuscularly (lower limb) for preoperation sedation after inducing anesthesia. After left thoracotomy was performed, the left anterior descending coronary artery was permanently ligated by 7–0 poly suture to induce AMI models. Infarction was visually assessed by regional cardiac cyanosis. The Sham-operated controls underwent all surgical procedures except the coronary artery ligated. All animal procedures were approved by the Animal Care Committee of the Shanxi Medical University. All experiments were carried out in accordance with the Guide for the Care and Use of Laboratory Animals (NIH, 8th Edition, 2011).

Fig. 1 Working flow of the study. AMI = acute myocardial infarction, OP = operation, preOP = pre-operation, pOP = post-operation, F = finalise. # Data from two groups of four rats on day 3 were used for histopathological pre-assessment
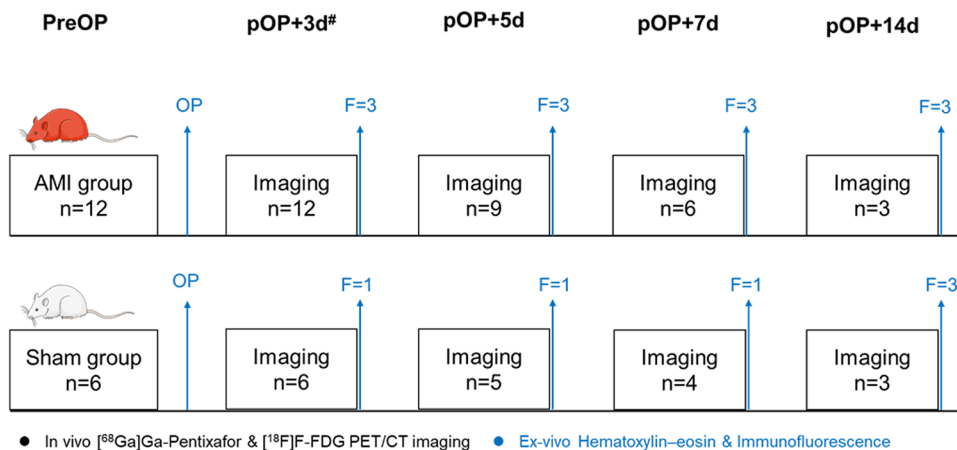
In vivo Cardiac PET/CT Imaging

Radiosynthesis of [68Ga]Ga-Pentixafor and [18F]F-FDG

[68Ga]Ga-Pentixafor was synthesized by the following steps. Firstly, 68Ga was eluted from 68Ge/68Ga generators, concentrated using a cation exchange cartridge, mixed with a solution of Pentixafor, and then heated at 100 °C (PH ~ 4) for 15 minutes. [68Ga]Ga-Pentixafor was purified using a C18 solid phase extraction cartridge, and then removed using ethanol/water. Lastly, chemical and radiochemical purity of [68Ga]Ga-Pentixafor was analyzed by high-performance liquid chromatograph (HPLC) system [21]. [18F]F-FDG was synthesized as previously described [22].

In-vivo Imaging

[68Ga]Ga-Pentixafor and [18F]F-FDG PET/CT scans were performed pre-operation and 5, 7, 14 days post-operation on a dedicated small-animal microPET/CT scanner (Inviscan, IRIS PET/CT, France). The anesthetization was conducted with 2 ~ 3% isoflurane and remained over the entire imaging. Rats were placed supine within the scanner. Heart rate, temperature and respiration were monitored continuously. [68Ga]Ga-Pentixafor static imaging was performed without special preparation. [18F]F-FDG gated imaging was performed 12 hours after [68Ga]Ga-Pentixafor imaging at each time-point, with rats fasted no less than 4 h. Additionally, the electrode pads were attached to dynamically monitor

cardiac cycle for function parameters assessment. [68Ga]Ga-Pentixafor (5.5 ± 1.7 MBq) or [18F]F-FDG (6.5 ± 2.1 MBq) were administered as a 0.10 to 0.15 ml bolus via the tail vein. A 10 min scan was acquired at 50 min after injection. The matrix size was $101 \times 101 \times 120$, voxel dimension was 0.85 mm, and field-of-view was 80 mm × 95 mm. All PET images were reconstructed using the 3D-ordered-subsets implementations-Monte Carlo algorithm, with 8 subsets and 8 iterations.

Imaging Analysis

Two experienced physicians in cardiac PET imaging visually assessed the PET/CT images and were in consensus for the image interpretation. The accumulation of [68Ga]Ga-Pentixafor and the cardiac function measured by [18F]F-FDG gated imaging were analyzed by Osirix Imaging Software (Version 3.5.1) and PMOD software (Version 4.1), respectively. The cardiac functional parameters included LV ejection fraction (LVEF), end-diastolic volume (EDV) and end-systolic volume (ESV). [18F]F-FDG imaging was also referred to locate the myocardium, and the defect of [18F]F-FDG uptake represented the infarct territory.

Briefly, $5 \sim 15$ mm^2 of appropriate regions of interest (ROIs) were manually brushed on infarcted (anterior apical wall, Fig. 2A) and remote (opposite and far away from the infarct area, like septum, inferior or lateral wall, Fig. 2B) myocardium to obtain mean and maximum standardized uptake value (SUVmean and SUVmax), respectively. The

Fig. 2 Quantitative analysis of [68Ga]Ga-Pentixafor imaging: delineation in the infarcted myocardium (**A**), remote myocadium (**B**), liver (**D**), and inflammation volume sketch layer by layer referred to [18F]F-FDG imaging (**C**)
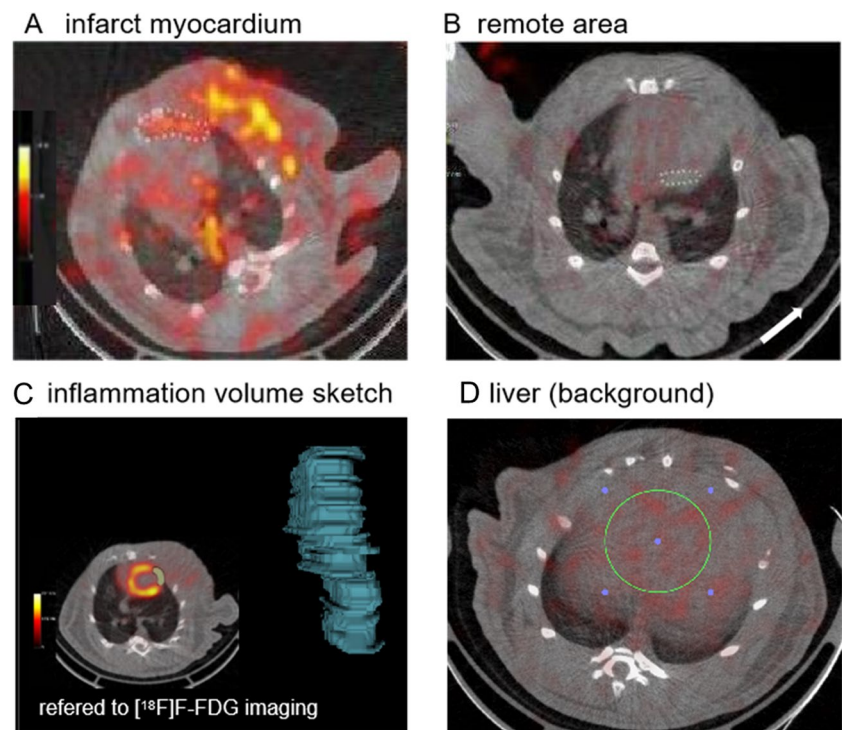
inflammatory volume was calculated by manually sketching the whole consecutive area with increased activity layer by layer, with a reference from the absent area in [^{18}F]F-FDG imaging (Fig. 2C). For background assessment, SUVmean of the middle liver parenchyma (a 1.0~2.0 cm^2 ellipse, Fig. 2D) were measured in view of the smaller heterogeneity in the liver activity inter-individuals and its high reproducibility. Of note, regions with large blood vessels or heavy respiratory artifacts were avoided. All ROIs were drawn on trans-axial PET images, and if necessary, were checked on trans-saggital and trans-coronal sections. For remote myocardium and liver, at least 3 consecutive layers of SUVmean were measured and then averaged as final. The target-to-background ratio (TBR) of [^{68}Ga]Ga-Pentixafor was calculated to correct the heterogenous background among rats by dividing SUVmax or SUVmean of myocardium by SUVmean of liver.

Ex-vivo Immunohistological Staining

At least three rats in AMI group and one rat in Sham group were finalised at each time point post operation. The hearts were harvested, fixed in 4% paraformaldehyde solution, and cut into 4 µm paraffin sections. All sections were stained with Hematoxylin–eosin (HE) to assess morphological changes and the infarct area in percentage in the largest infarct section. The latter was determined by mean value of three successive layers of sections of the infarct central area.

To illustrate the pathological change of the PET activity, the dynamic evolution of polarized M1/M2-macrophages was semi-quantified by immunofluorescence double staining. CD68 staining (green) was used to identify macrophages, and further iNOS/CD206 counterstaining (red) to identify M1/M2-macrophages. DAPI staining (blue) was to identify nuclei. Briefly, sections were deparaffinized and rehydrated through a series of xylene and graded alcohols. Then, antigen retrieval was performed by EDTA buffer

(PH = 9). After blocking (5% bovine serum albumin in PBS) for 30 min at room temperature, sections were incubated overnight with the primary antibody including mouse-anti CD68 (Invitrogen, 1:100), rat-anti iNOS (Invitrogen, 1:100), and rabbit-anti CD206 (Invitrogen, 1:100) at 4 °C. The secondary antibody incubated for 1 h at room temperature with anti-mouse IgG Alexa Fluor™ 488, anti-rat IgG Alexa Fluor™ Plus 594, and anti-rabbit IgG Alexa Fluor™ Plus 555 (Invitrogen, 1:500). Immunofluorescence microscopy (Ti-U, Nicon, Japan) was used to visualize sectional images. Images were obtained from each slide using ×20 objective. ImageJ software (version 1.8.0 National Institutes of Health, Bethesda, MD, USA) was used to analyze M1/M2-macrophages positivity and infarct area in percentage.

Statistical Analysis

Statistical analysis was performed using SPSS statistics 25 (IBM Corp.). Kolmogorov–Smirnov testing was explored to observe the data normality. Continuous variables are expressed as mean ± SD. Comparisons between AMI and Sham groups at individual time points were performed with Mann-Whitney U-test. Correlations of [^{68}Ga]Ga-Pentixafor uptake in different myocardial region, [^{68}Ga]Ga-Pentixafor uptake with the size of inflammation area, parameters of cardiac function, and percentage of M1/M2 macrophages were analyzed by Pearson correlation analysis. A two-tailed P value < 0.05 was considered statistically significant.

Results

The Longitudinal Cardiac Function by [^{18}F]F-FDG Imaging

As illustrated in Fig. 3 and Table 1, LVEF was significantly dropped at day 5 early after AMI versus the Sham group
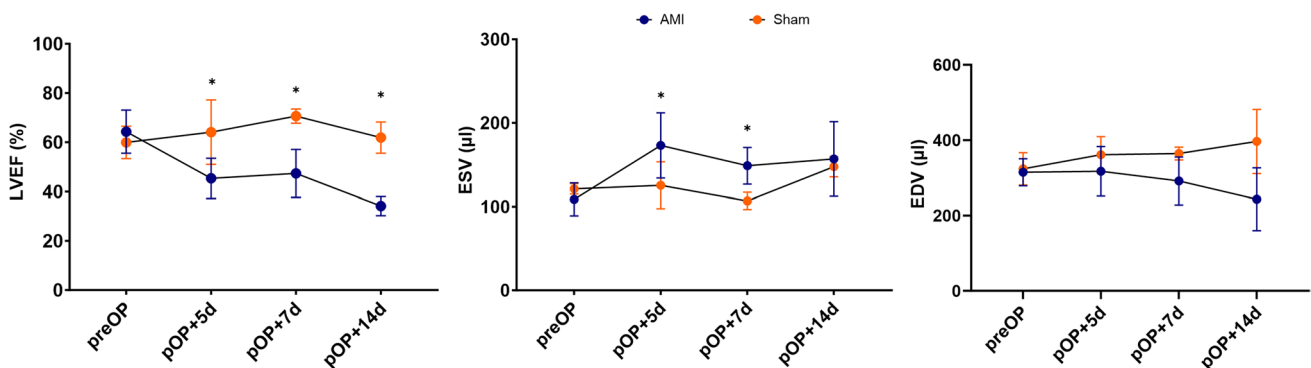

Fig. 3 Longitudinal evolution of cardiac function post-operation. AMI vs Sham: * $P < 0.05$, ** $P < 0.01$. AMI = acute myocardial infarction, preOP = pre-operation, pOP = post-operation

Table 1 Comparison of Cardiac Function between Groups

	preOP		pOP+5d		pOP+7d		pOP+14d	
	AMI	Sham	AMI	Sham	AMI	Sham	AMI	Sham
LVEF(%)	64.30 ± 8.77	59.90 ± 6.58	45.34 ± 8.14*	64.10 ± 13.08	47.34 ± 9.72*	70.63 ± 2.89	34.12 ± 3.87*	61.88 ± 6.32
EDV(μl)	314.47 ± 35.86	323.65 ± 42.99	317.09 ± 65.72	361.09 ± 48.28	291.39 ± 63.53	364.27 ± 17.20	242.94 ± 83.12	396.31 ± 85.26
ESV(μl)	108.61 ± 19.65	121.17 ± 6.18	173.03 ± 38.94*	125.40 ± 27.94	148.75 ± 21.87*	106.83 ± 10.38	156.93 ± 44.57	147.65 ± 12.16

AMI vs Sham: * $P < 0.05$. *LVEF* left ventricular ejection fraction, *EDV* end-diastolic volume, *ESV* end-systolic volume, *preOP* pre-operation, *pOP* post-operation, *AMI* acute myocardial infarction

($45.34 \pm 8.14\%$ vs. $64.10 \pm 13.08\%$, $P = 0.028$), and deteriorated over 14 days ($34.12 \pm 3.87\%$ vs. $61.88 \pm 6.32\%$, $P = 0.049$). ESV significantly elevated in AMI group around 1 week after AMI (day 5: $173.03 \pm 38.94 \, \mu l$ vs. $125.40 \pm 27.94 \, \mu l$, $P = 0.039$; day 7: $148.75 \pm 21.87 \, \mu l$ vs. $106.83 \pm 10.38 \, \mu l$, $P = 0.011$). There was no significant difference of EDV between groups ($P > 0.05$).

The Longitudinal Evolution of [^{68}Ga]Ga-Pentixafor Imaging

The uptake evolution of [^{68}Ga]Ga-Pentixafor in the two groups was shown in Fig. 4 and Table 2. For the infarcted myocardium, both SUV and TBR of [^{68}Ga]Ga-Pentixafor

peaked on day 5 after AMI (all $P = 0.003$), retained on day 7 (all $P = 0.011$), and gradually declined until 14 days ($P > 0.05$). The typical images of one AMI rat were shown in Fig. 5. The volume of the inflammatory area was largest at day 5 and gradually reduced at day 7 and 14 after AMI ($P = 0.011$). Both SUV (SUVmean: $r = 0.815$, $P < 0.001$; SUVmax: $r = 0.711$, $P = 0.001$) and TBR (TBRmean: $r = 0.731$, $P = 0.001$; TBRmax: $r = 0.613$, $P = 0.007$) in the infarct area was positively correlated with the inflammatory volume.

For the remote myocardium, significantly elevated activity of [^{68}Ga]Ga-Pentixafor on day 5 (AMI vs. Sham: SUVmean: 0.14 ± 0.03 vs. 0.07 ± 0.04, $P = 0.016$; SUVmax: 0.20 ± 0.04 vs. 0.11 ± 0.04, $P = 0.005$; TBRmean:
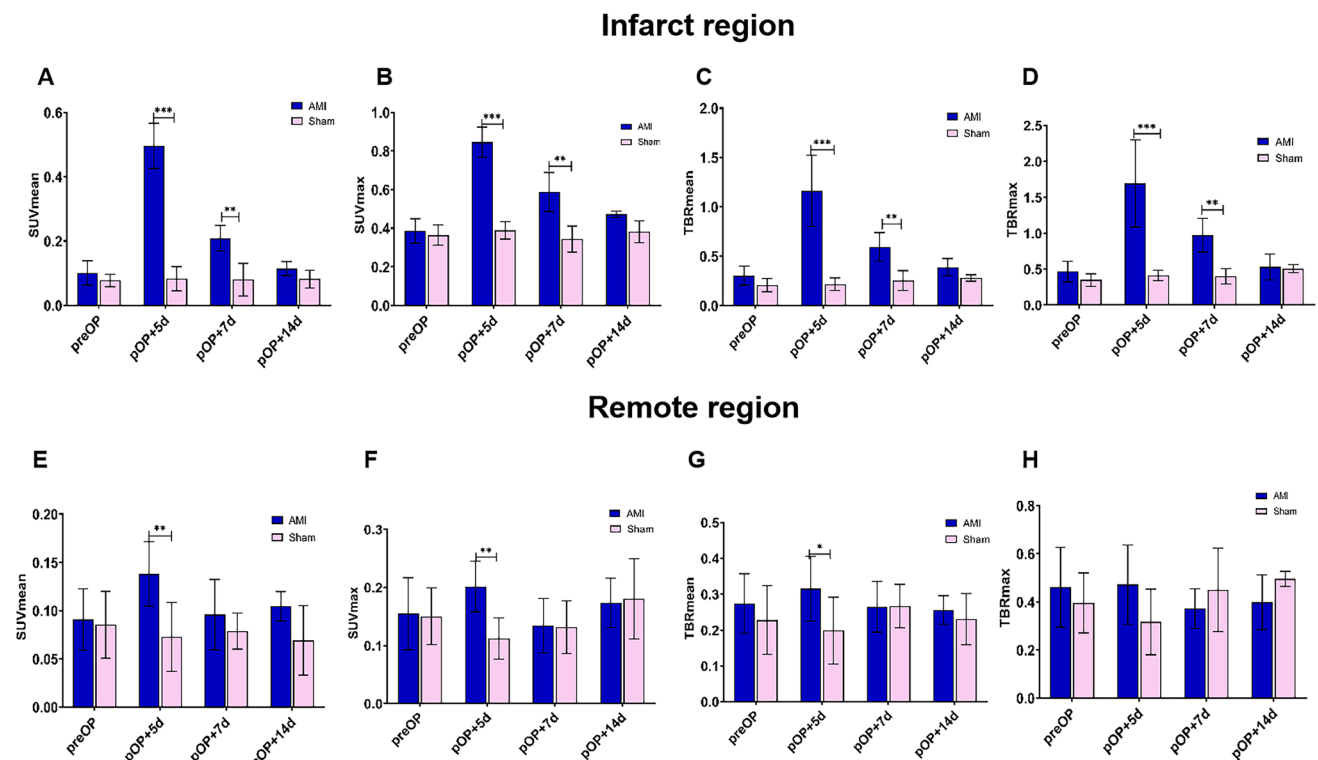

Fig. 4 Longitudinal evolution of [^{68}Ga]Ga-Pentixafor uptake in the infarct (**A-D**) and remote (**E-H**) area. AMI vs sham: * $P < 0.05$, ** $P < 0.01$. AMI = acute myocardial infarction, preOP = pre-operation, pOP = post-operation

Table 2 Longitudinal Evolution of [^{68}Ga]Ga-Pentixafor Uptake in the Infarct and Remote Myocardium

Time Point	Group	Evaluated Area	SUVmean	SUVmax	TBRmean	TBRmax
preOP	AMI	LV myocardium	0.10 ± 0.03	0.15 ± 0.05	0.29 ± 0.09	0.46 ± 0.15
	Sham		0.09 ± 0.03	0.15 ± 0.05	0.23 ± 0.10	0.37 ± 0.10
pOP+5d	AMI	Infarct	0.50 ± 0.07**	0.72 ± 0.13**	1.30 ± 0.28**	1.90 ± 0.47**
		Remote	0.14 ± 0.03*	0.20 ± 0.04**	0.36 ± 0.08*	0.53 ± 0.14
	Sham	LV myocardium	0.07 ± 0.04	0.13 ± 0.04	0.21 ± 0.09	0.36 ± 0.14
pOP+7d	AMI	Infarct	0.21 ± 0.04*	0.35 ± 0.12*	0.59 ± 0.10*	0.97 ± 0.23*
		Remote	0.10 ± 0.04	0.13 ± 0.05	0.27 ± 0.07	0.37 ± 0.08
	Sham	LV myocardium	0.08 ± 0.03	0.13 ± 0.05	0.26 ± 0.07	0.43 ± 0.15
pOP+14d	AMI	Infarct	0.17 ± 0.02	0.22 ± 0.02	0.39 ± 0.09	0.53 ± 0.18
		Remote	0.14 ± 0.04	0.17 ± 0.04	0.33 ± 0.11	0.40 ± 0.11
	Sham	LV myocardium	0.07 ± 0.04	0.16 ± 0.07	0.26 ± 0.07	0.58 ± 0.20

AMI vs Sham: * $P < 0.05$, ** $P < 0.01$. *preOP* pre-operation, *pOP* post-operation, *SUV* standard uptake value, *TBR* target background ratio, *AMI* acute myocardial infarction, *LV* left ventricular
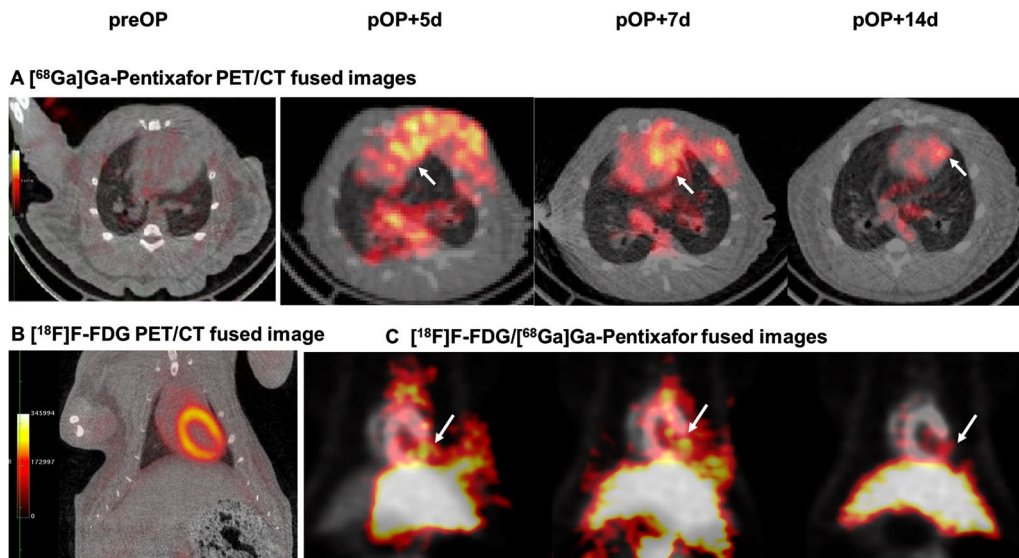

Fig. 5 Typical evolution images of an AMI rat. (**A**) [^{68}Ga]Ga-Pentixafor PET/CT fused images pre- and post- AMI; (**B**) [^{18}F]F-FDG PET/CT fused image pre-AMI; (**C**) [^{18}F]F-FDG/[^{68}Ga]Ga-Pentixafor fused images post-AMI. The white arrow indicated the myocardial infarction area. preOP = pre-operation, pOP = post-operation

0.32 ± 0.09 vs. 0.20 ± 0.09, $P = 0.023$) after AMI were observed, correlating with the contemporaneous SUVmean ($r = 0.688$, $P = 0.04$) and TBRmean ($r = 0.868$, $P = 0.002$) in the infarct territory. The activity in the remote myocardium began to recover from day 7 (AMI vs. Sham: $P > 0.05$). Of note, SUVmean in the remote region of [^{68}Ga]Ga-Pentixafor on day 5 after AMI negatively correlated with contemporaneous EDV ($r = -0.826$, $P = 0.006$) and ESV ($r = -0.821$, $P = 0.007$), additionally, TBRmean in the remote region was also correlated with contemporaneous EDV ($r = -0.667$, $P = 0.049$). No correlation of uptake intensity of remote myocardium was found with the inflammation area and cardiac functional parameters at other time points ($P > 0.05$). No difference of [^{68}Ga]

Ga-Pentixafor uptake was detected on serial imaging in Sham group.

Associations Between Macrophages and [^{68}Ga]Ga-Pentixafor Activity

AMI groups showed disorderly myocardial fibers with myocardial cells necrosis and inflammatory cell infiltration in the infarct region (Fig. 6). The infarct area in percentage determined by HE staining was $18 \pm 2\%$.

Immunofluorescence images are shown in Fig. 7A, Macrophage infiltration in the infarcted myocardium was dramatically increased and peaked approximately at day 5 after AMI, with pro-inflammatory M1-macrophages

Fig. 6 HE staining of myocardial tissue in Sham (**A**) and AMI (**B**) rats 3 days after operation
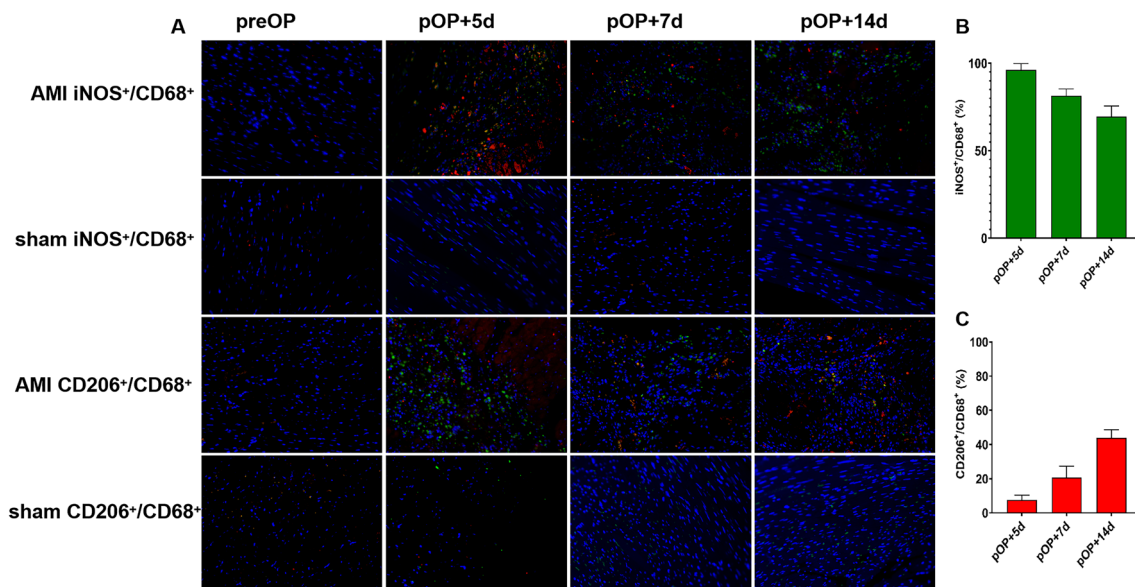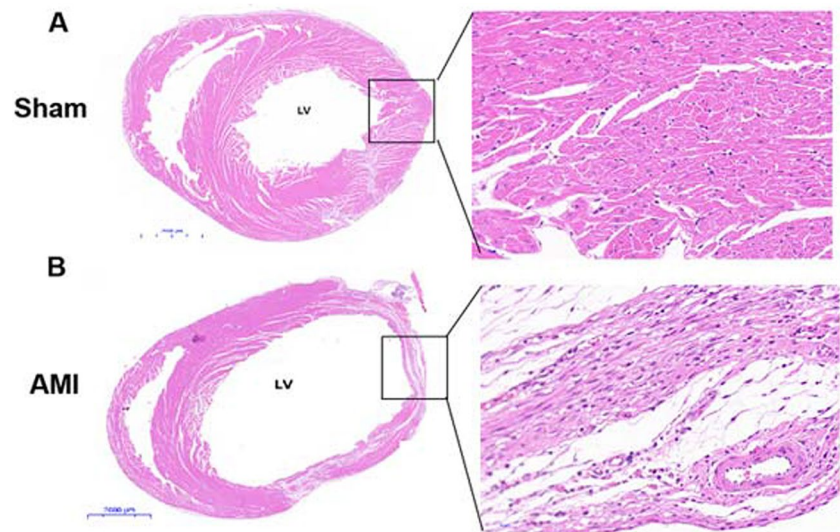

Fig. 7 Longitudinal evolution of M1/M2-macrophages: (**A**) Typical immunofluorescent double-stained pictures of M1/M2-macrophages in the AMI and Sham groups pre- and post-surgery; (**B**) Percent of M1-macrophages in AMI group; (**C**) Percent of M2-macrophages in AMI group. iNOS+/CD68+ and CD206+/CD68+ represent M1 and M2 macrophages, respectively

predominating (Fig. 7B). As pro-inflammatory M1-macrophages decreased, the proportion of M2-macrophages progressively increased over 14 days (Fig. 7C).

There were strong correlations between [^{68}Ga]Ga-Pentixafor activity and percentage of M1/M2 macrophages (M1: $P < 0.05$; M2: $P < 0.01$). The tendency of [^{68}Ga]Ga-Pentixafor evolution was consistent with the rise-fall M1 macrophages (SUVmean: $r = 0.870$, $P = 0.002$; SUVmax: $r = 0.921$, $P < 0.001$; TBRmean: $r = 0.780$, $P = 0.013$; TBRmax: $r = 0.829$, $P = 0.006$). Furthermore, the inflammatory area of [^{68}Ga]Ga-Pentixafor was correlated with

both M1 and M2 macrophages (M1: $r = 0.811$, $P = 0.008$; M2: $r = -0.880$, $P = 0.002$).

Discussion

Previous molecular imaging studies have exemplified that persistent pro-inflammatory response in the infarct area after AMI can contribute to adverse LV remodelling and heart failure [7]. Our study demonstrated that the [^{68}Ga]Ga-Pentixafor inflammatory activity elevated significantly

at 5 days after AMI in both the infarcted and remote regions and then gradually decreased. In addition, an association between radioactivity in the remote area and LV remodeling was initially observed in our experiments. Ex-vivo tissue work-up confirmed a corresponding evolutionary trend of pro-inflammatory M1-macrophages in the infarct area.

The orchestrated recruitment transition from proinflammatory to reparative cell may mitigate AMI injury, promote repair, and improve prognosis [2, 23], *in vivo* non-invasive monitoring of these processes is important for selecting the appropriate timing and intervention protocol. The CANTOS trial and a large body of clinical trials followed in patients with AMI have proved this [23, 24]. Currently, the application of [^{68}Ga]Ga-Pentixafor in AMI is in the most initial stage. To the best of our knowledge, only single-digit relevant original articles have been published currently. Studies remain pending regarding the dynamic evolution of CXCR4-inflammatory response, clinical significance of the radioactive activity, the interaction between organs, as well as the therapeutic guidance potentials.

Regarding the prognostic value of [^{68}Ga]Ga-Pentixafor activity in the infarcted myocardium, inconsistencies occurred in the animal and clinical studies currently. For example, Reiter et al. enrolled 13 patients 2–13 days post-AMI, and revealed that the higher the [^{68}Ga]Ga-Pentixafor activity, the smaller the following scar volumes [25]. Yet, Hess et al. demonstrated that persistently high [^{68}Ga]Ga-Pentixafor activity in the infarct zone within 3 days predict a higher incidence of acute LV rupture and chronic contractile dysfunction [13]. Preliminary intervention trials found that an opportune inflammation blocking (early after infarction) produce a positive outcome [13], whereas blocking at an inappropriate timing (depletion of macrophages prior to AMI) will aggravate a poor prognosis [26]. These have raised the demand for longitudinally in-vivo inflammatory characterization, the success of inflammation-targeted therapy largely depends on the appropriate target cells and timing.

Integrated from previous results, the [^{68}Ga]Ga-Pentixafor activity of the infarcted myocardium surged immediately after surgery, peaked approximately at day 3, and decreased visibly after 7 days [19, 27]. The persistency of [^{68}Ga]Ga-Pentixafor activity after AMI is shorter than [^{18}F]F-FDG, the latter can persist to at least 14 days after AMI [11]. The evolution of [^{68}Ga]Ga-Pentixafor activity observed in our study was comparable to previous results, with the following updates. Firstly, previous studies used the remote region as a background for uptake correction of interindividual heterogeneity, however, this is probably not the optimal choice. According to previous studies, severe inflammatory response may affect the remote area and even the kidney [6, 27], whereas [^{68}Ga]Ga-Pentixafor uptake in the liver is relatively stable [28]. Therefore, in the current study, the liver

was used as the site for background correction, which may objectively reflect the evolution of inflammatory activity in the non-infarcted area. Secondly, the [^{68}Ga]Ga-Pentixafor activity almost recovered to baseline on day 7 post-infarction in previous studies. Yet, in our study, although the [^{68}Ga]Ga-Pentixafor activity in the infarct area was reduced on day 7 versus day 5 post-AMI, it remained significantly higher than that in the Sham group, which was consistent with the ex-vivo autoradiography results on day 7 by Hess et al. They concluded that the higher sensitivity and lack of background activity with autoradiography result in the positive results [13]. Besides, the correction using the activity in the remote area might be another speculation. Our results may further justify the correct choice of using the liver as a background [19, 27, 28]. Third, previous studies have mostly set time points of 3 days, 7 days, and 6 weeks post-AMI for assessment, we set 2 extra time points at 5 days and 14 days after AMI, filling the gap of [^{68}Ga]Ga-Pentixafor evolution in previous studies. Regarding the clinical translation in future, the extended time window may implicate more feasibilities in patients monitoring after AMI. Furthermore, the back-to-baseline (significance lost) activity at 14 days after AMI can be considered as the end of the early surged inflammatory activity after AMI in rodents, which has not been clarified in previous [^{68}Ga]Ga-Pentixafor studies. Fourth, Hess et al. found the early (1 and 3 days after AMI) CXCR4 activity in the infarct area correlated well with subsequent LVEF, however, the correlation at day3 days started to get weakened [13]. It can be speculated that the correlation will further weaken with time. The temporal bias of monitoring (relatively later) might be an explanation of the absent correlation between [^{68}Ga]Ga-Pentixafor activity post-operation and LVEF in the present study.

Regarding the prognostic value of remote area, previous [^{18}F]F-FDG inflammatory imaging studies indicated controversial [^{18}F]F-FDG activity elevated in the remote myocardium [6, 10, 11]. Wollenweber et al. detected increased [^{18}F]F-FDG uptake in the non-infarcted area, spleen and bone marrow of AMI patients [10]. However, a recent study by Xi et al. in infarcted pigs did not observe a meaningful increase in [^{18}F]F-FDG uptake in the non-infarcted region [11]. In a mice and clinical study by Werner et al., [^{68}Ga]Ga-Pentixafor activity in the infarcted and remote myocardium were both correlated with the activity in the kidney, moreover, the remote activity in AMI patients within 4 days of reperfusion was the only independent predictor of renal events [27]. However, none of aforementioned studies focus on the dynamic evolution and predictive value of [^{68}Ga]Ga-Pentixafor activity in the remote region. Our study preliminarily displayed the longitudinal [^{68}Ga]Ga-Pentixafor evolution in the remote area after AMI, and observed the capacity of [^{68}Ga]Ga-Pentixafor in detecting the unobtrusively increased inflammation in the remote myocardium

early after AMI, as well as its potential value in predicting cardiac remodelling, which lays the foundation for further prognostic studies in the future.

As for the predictive mechanisms of the activity in the remote region, firstly, spreading of the severe inflammatory response from the infarct area to the non-infarct area was concerned an established mechanism [6]. Secondly, abnormal first-pass perfusion or reduced microcirculatory reserve (ie. coronary flow reserve) were also identified in the non-infarct area following revascularization in AMI patients [29, 30]. Our previous clinical observational research also identified the presence of coronary microvascular disease in the non-obstructed coronary territory in patients with obstructive coronary artery disease [31]. Furthermore, amplification of extracellular matrix, upregulated matrix metalloproteinases, systolic dysfunction, and thinning of the ventricular wall were also observed in the remote myocardium after AMI, all of which may be associated with poor prognosis.

Regarding the type of inflammatory cells targeted by [68Ga]Ga-Pentixafor, an *in-vitro* study confirmed a broad [68Ga]Ga-Pentixafor accumulation in monocytes/macrophages and lymphocytes, and for the former, comparable uptake was observed in M1- and M2-polarized macrophages [32]. Our in-vivo studies clarified a strong rise-fall parallel between [68Ga]Ga-Pentixafor accumulation and infiltrated M1-macrophages in infarct territory, despite there was also a correlation between M2-macrophages and [68Ga]Ga-Pentixafor accumulation. Thus, here it can be speculated that pro-inflammatory M1-macrophages attributed more to the subsequent cardiac dysfunction or adverse remodelling. Regarding the observed profitably predictive value of [68Ga]Ga-Pentixafor in AMI patients by Reiter et al. [25], the relatively later monitoring time-frame possibly reflected mainly reparative inflammatory cells, exactly as the significantly increased M2-macrophages percent around day 7–14 after AMI we observed. The controversial correspondence between macrophage phenotype and [68Ga]Ga-Pentixafor in-vivo and ex-vivo may attribute to multi-factors including species characteristics, diverse assessing time point, and heterogeneity among individuals, which warrant further studies.

Given broad spectrum of leukocytes identified by [68Ga]Ga-Pentixafor, the research for more specific radiotracers is ongoing. So far, large amount of neuro-inflammatory research reflected [18F]F-GE-180 that targets translocator protein (TSPO) as a novel better PET radiotracer than [11C]C-R-PK11195, which markedly identify M1-macrophages [33]. Over recent years, novel promising tracer such as [68Ga]Ga-mCXCL12, [68Ga]Ga-DOTATATE, and [68Ga]Ga-DOTA-ECL1i allosterically binding to CCR2 performed a potentially valid assessment in cardiovascular inflammation [34]. More work is needed to validate the value of these novel radiotracers in guiding theranostics of cardiovascular disease.

Limitations

Certain noticeable limitations of our study need to be acknowledged. The first major limitation concerns the small sample size, which constrained to further explore the relevant association at various time points, and conclusions should be drawn prudently. Further verification needs to be confirmed in large samples. Second, our work has not yet carried out an explanation for the prognostic mechanism, i.e., no in-depth histological studies have been conducted to quantify the evolution of macrophages more precisely, the cell origin and the gradient distribution in infarct regions. Third, we did not perform blocking experiments towards [68Ga]Ga-Pentixafor activity and observe its longer-term change as well. For the infarct area, Hess et al. have shown that early [68Ga]Ga-Pentixafor activity can predict chronic contractile dysfunction at 6 weeks [13]. For the remote myocardium, due to non-significant difference in activity between the AMI and Sham groups at day 7 and day 14, further assessment was not necessarily conducted. Fourth, we used gated [18F]F-FDG metabolic imaging than the gold criteria cardiac magnetic resonance imaging (CMRI) to evaluate the cardiac function, which may trigger questioning. However, prior comparative study has proved an excellent agreement of cardiac function between gated [18F]F-FDG and CMRI [29], additionally, we eliminated the outlier values in the parameters of cardiac function, which may compensate for the deficiency.

Conclusions

Corresponding with the peaked [68Ga]Ga-Pentixafor activity in the infarcted myocardium, the activity in the remote region also elevated accordingly and led to left ventricular remodelling early after AMI, which was attributed to the early surged pro-inflammatory response. Further studies concerning the remote myocardium are warranted to clarify the post-inflammation mechanism and the clinical application potential.

Declarations

Conflict of Interests None of the authors have anything to disclose.

Disclosures The authors have no conflict of interest and nothing to disclose.

References

1. Virani SS, Alonso A, Aparicio HJ et al (2021) American Heart Association Council on epidemiology and prevention statistics committee and stroke statistics subcommittee. Heart disease and stroke Statistics-2021 update: a report from the American Heart Association. Circulation 143(8):e254–e743

2. Ong SB, Hernández-Reséndiz S, Crespo-Avilan G et al (2018) Inflammation following acute myocardial infarction: multiple players, dynamic roles, and novel therapeutic opportunities. Pharmacol Ther 186:73–87

3. Matter MA, Paneni F, Libby P et al (2024) Inflammation in acute myocardial infarction: the good, the bad and the ugly. Eur Heart J 45(2):89–103

4. Cerisano G, Buonamici P, Valenti R et al (2014) Early short-term doxycycline therapy in patients with acute myocardial infarction and left ventricular dysfunction to prevent the ominous progression to adverse remodelling: the TIPTOP trial. Eur Heart J 35(3):184–191

5. Hess A, Derlin T, Koenig T et al (2020) Molecular imaging-guided repair after acute myocardial infarction by targeting the chemokine receptor CXCR4. Eur Heart J 41(37):3564–3575

6. Lee WW, Marinelli B, van der Laan AM et al (2012) PET/MRI of inflammation in myocardial infarction. J Am Coll Cardiol 59(2):153–163

7. Westman PC, Lipinski MJ, Luger D et al (2016) Inflammation as a driver of adverse left ventricular remodeling after acute myocardial infarction. J Am Coll Cardiol 67(17):2050–2060

8. Celiker-Guler E, Ruddy TD, Wells RG (2021) Acquisition, processing, and interpretation of PET 18F-FDG viability and inflammation studies. Curr Cardiol Rep 23(9):124

9. Fischer M, Zacherl MJ, Weckbach L et al (2021) Cardiac 18F-FDG positron emission tomography: an accurate tool to monitor *in vivo* metabolic and functional alterations in murine myocardial infarction. Front Cardiovasc Med 8:656742

10. Wollenweber T, Roentgen P, Schäfer A et al (2014) Characterizing the inflammatory tissue response to acute myocardial infarction by clinical multimodality noninvasive imaging. Circ Cardiovasc Imaging 7(5):811–818

11. Xi XY, Zhang F, Wang J et al (2020) Functional significance of post-myocardial infarction inflammation evaluated by 18F-fluorodeoxyglucose imaging in swine model. J Nucl Cardiol 27(2):519–531

12. Zhou W, Guo S, Liu M et al (2019) Targeting CXCL12/CXCR4 Axis in tumor immunotherapy. Curr Med Chem 26(17):3026–3041

13. Chen Z, Xue Q, Huang C et al (2022) Burkitt lymphoma/leukemia presented on 68Ga-Pentixafor and 18F-FDG PET/CT. Clin Nucl Med 47(1):98–100

14. Pan Q, Cao X, Luo Y et al (2020) Chemokine receptor-4 targeted PET/CT with 68Ga-Pentixafor in assessment of newly diagnosed multiple myeloma: comparison to 18F-FDG PET/CT. Eur J Nucl Med Mol Imaging 47(3):537–546

15. Herhaus P, Habringer S, Philipp-Abbrederis K et al (2016) Targeted positron emission tomography imaging of CXCR4 expression in patients with acute myeloid leukemia. Haematologica 101(8):932–940

16. Galsky MD, Vogelzang NJ, Conkling P et al (2014) A phase I trial of LY2510924, a CXCR4 peptide antagonist, in patients with advanced cancer. Clin Cancer Res 20(13):3581–3588

17. Herrmann K, Schottelius M, Lapa C et al (2016) First-in-human experience of CXCR4-directed Endoradiotherapy with 177Lu- and 90Y-labeled Pentixather in advanced-stage multiple myeloma with extensive intra- and Extramedullary disease. J Nucl Med 57(2):248–251

18. Li X, Yu W, Wollenweber T et al (2019) [68Ga]Pentixafor PET/MR imaging of chemokine receptor 4 expression in the human carotid artery. Eur J Nucl Med Mol Imaging 46(8):1616–1625

19. Thackeray JT, Derlin T, Haghikia A et al (2015) Molecular imaging of the chemokine receptor CXCR4 after acute myocardial infarction. JACC Cardiovasc Imaging 8(12):1417–1426

20. Pan D, Xu YP, Yang RH et al (2014) A new (68)Ga-labeled BBN peptide with a hydrophilic linker for GRPR-targeted tumor imaging. Amino Acids 46(6):1481–1489

21. Krasikova R (2007) Synthesis modules and automation in F-18 labeling. Ernst Schering Res Found Workshop 62:289–316

22. Döring Y, Pawig L, Weber C et al (2014) The CXCL12/CXCR4 chemokine ligand/receptor axis in cardiovascular disease. Front Physiol 5:212

23. Huang S, Frangogiannis NG (2018) Anti-inflammatory therapies in myocardial infarction: failures, hopes and challenges. Br J Pharmacol 175(9):1377–1400

24. Ridker PM, Everett BM, Thuren T et al (2017) Antiinflammatory therapy with Canakinumab for atherosclerotic disease. N Engl J Med 377(12):1119–1131

25. Reiter T, Kircher M, Schirbel A et al (2018) Imaging of C-X-C motif chemokine receptor CXCR4 expression after myocardial infarction with [68Ga]Pentixafor-PET/CT in correlation with cardiac MRI. JACC Cardiovasc Imaging 11(10):1541–1543

26. Hess A, Borchert T, Ross TL et al (2022) Characterizing the transition from immune response to tissue repair after myocardial infarction by multiparametric imaging. Basic Res Cardiol 117(1):14

27. Werner RA, Hess A, Koenig T et al (2021) Molecular imaging of inflammation crosstalk along the cardio-renal axis following acute myocardial infarction. Theranostics 11(16):7984–7994

28. Herrmann K, Lapa C, Wester HJ et al (2015) Biodistribution and radiation dosimetry for the chemokine receptor CXCR4-targeting probe 68Ga-pentixafor. J Nucl Med 56(3):410–416

29. Bethke A, Shanmuganathan L, Andersen GØ et al (2019) Microvascular perfusion in infarcted and remote myocardium after successful primary PCI: angiographic and CMR findings. Eur Radiol 29(2):941–950

30. Van Herck PL, Paelinck BP, Haine SE et al (2013) Impaired coronary flow reserve after a recent myocardial infarction: correlation with infarct size and extent of microvascular obstruction. Int J Cardiol 167(2):351–356

31. Wu P, Guo XS, Zhang X et al (2020) Value of absolute quantification of myocardial perfusion by PET in detecting coronary microvascular disease in patients with non-obstructive coronaries. Zhonghua Xin Xue Guan Bing Za Zhi 48(3):205–210

32. Borchert T, Beitar L, Langer LBN et al (2021) Dissecting the target leukocyte subpopulations of clinically relevant inflammation radiopharmaceuticals. J Nucl Cardiol 28(4):1636–1645

33. Boutin H, Murray K, Pradillo J et al (2015) 18F-GE-180: a novel TSPO radiotracer compared to 11C-R-PK11195 in a preclinical model of stroke. Eur J Nucl Med Mol Imaging 42(3):503–511

34. Heo GS, Kopecky B, Sultan D et al (2019) Molecular imaging visualizes recruitment of inflammatory monocytes and macrophages to the injured heart. Circ Res 124(6):881–890

Authors and Affiliations

Ping Wu[1,2] · Li Xu[1,2] · Qi Wang[3] · Xiaofang Ma[1] · Xinzhu Wang[3] · Hongliang Wang[1,2] · Sheng He[4] · Huibin Ru[1,2] · Yuting Zhao[1] · Yuxin Xiao[1] · Jingying Zhang[1] · Xinchao Wang[2] · Shaohui An[2,5] · Marcus Hacker[6] · Xiang Li[6] · Xiaoli Zhang[7] · Yuetao Wang[8] · Minfu Yang[9] · Zhifang Wu[1,2] · Sijin Li[1,2]

✉ Sijin Li
lisjnm123@163.com

Ping Wu
wuping_0815@163.com

1 Department of Nuclear Medicine, First Hospital of Shanxi Medical University, No. 85 Jiefang South Road, Taiyuan 030001, Shanxi, China

2 Collaborative Innovation Center for Molecular Imaging of Precision Medicine, Shanxi Medical University, Taiyuan, China

3 Department of Biochemistry and Molecular Biology, School of Basic Medicine, Shanxi Medical University, Taiyuan, China

4 Department of Radiology, First Hospital of Shanxi Medical University, Taiyuan, China

5 Shanghai United Imaging Healthcare Co., Ltd., Shanghai, China

6 Division of Nuclear Medicine, Department of Biomedical Imaging and Image-Guided Therapy, Medical University of Vienna, Vienna, Austria

7 Laboratory for Molecular Imaging, Department of Nuclear Medicine, Beijing Anzhen Hospital, Capital Medical University, Beijing, China

8 Department of Nuclear Medicine, The Third Affiliated Hospital of Soochow University, Changzhou, Jiangsu, China

9 Department of Nuclear Medicine, Beijing Chaoyang Hospital, Capital Medical University, Beijing, China